



DIFU<sub>100</sub>ci@

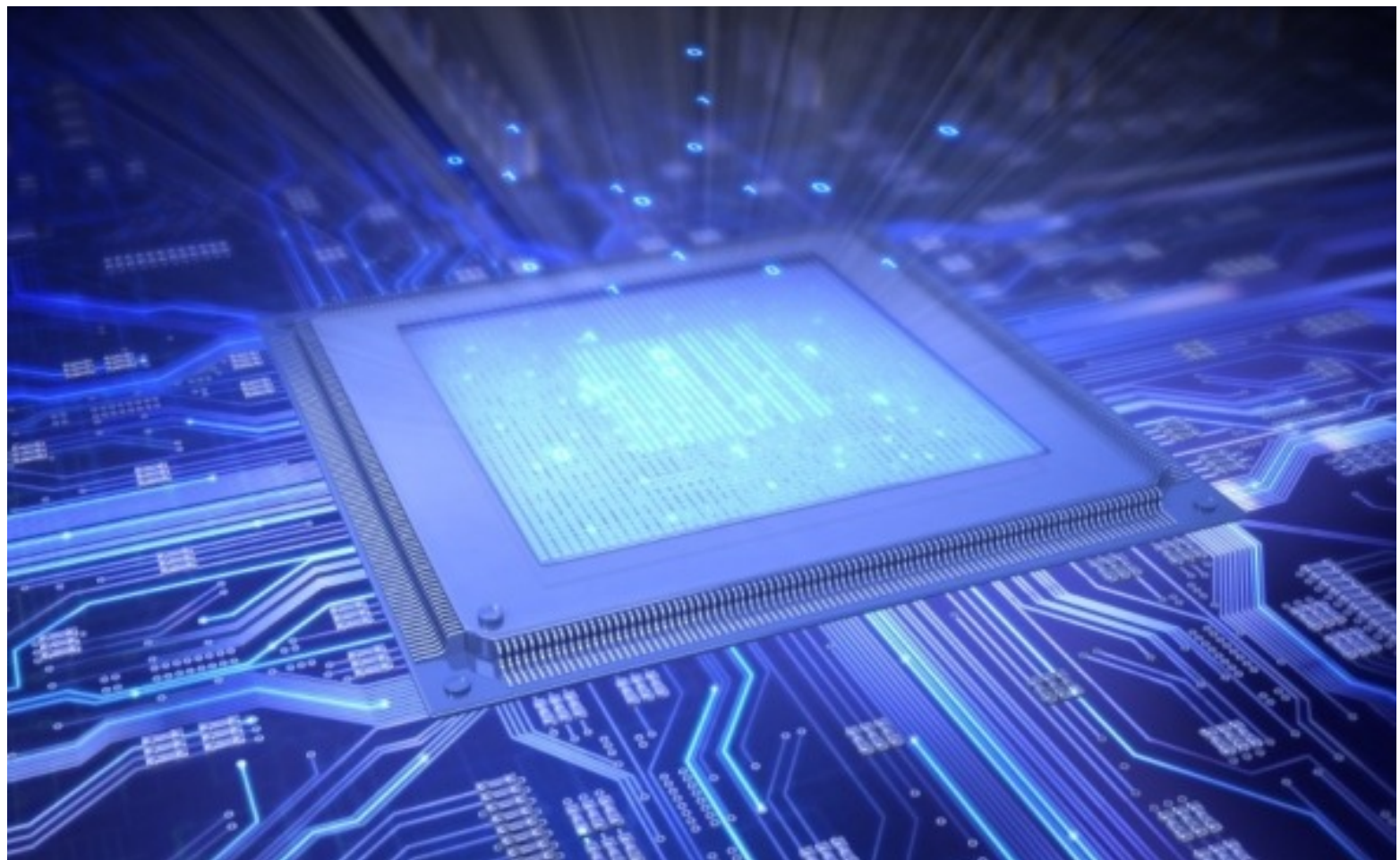
REVISTA DE DIFUSIÓN CIENTÍFICA  
INGENIERÍA Y TECNOLOGÍAS

ISSN 2007-3585

UAZ Universidad  
Autónoma de  
Zacatecas  
"Francisco García Salinas"



Vol. 7, No.3, enero-abril 2014



ISSN 2007-3585



PRODUCCIÓN

**Universidad Autónoma de Zacatecas**

PRODUCCIÓN Y DISEÑO

**Jorge Flores Troncoso**

D.R. de la Presente Edición

**Jorge Flores Troncoso**

**Universidad Autónoma de Zacatecas**

**López Velarde 801, Centro**

**98010 Zacatecas, Zac. México**

**ISSN 2007-3585**

DIFU100ci@ (léase difuciencia) Vol. 7, No.3, enero-abril 2014, es una publicación cuatrimestral editada por la Universidad Autónoma de Zacatecas, "Francisco García Salinas", Jardín Juárez 147, Col. Centro Zacatecas, Zac. C.P. 98000. <http://www2.uaz.edu.mx/web/www/publicaciones>. email: [jflorest@uaz.edu.mx](mailto:jflorest@uaz.edu.mx). Reservas de Derechos al Uso Exclusivo del Título expedido por el INDAUTOR, Reserva: 04-2010-110314331900-102. Responsable de la última actualización Jorge Flores Troncoso, López Velarde 801, Zona Centro, Zacatecas, Zac. C.P. 98000. Fecha de última modificación 30 de abril de 2014.

Hecho en México  
Made in Mexico

### **Directorio**

I. Q. Armando Silva Cháirez Rector  
Lic. Cuauhtémoc Rodríguez Aguirre Secretario General  
Dr. Miguel Rodríguez Jáquez Secretario Académico  
M. en A Emilio Morales Vera Secretario Administrativo  
Dr. Marco Antonio Salas Luévano Coord. Investigación y Posgrado  
Dra. Georgia Aralu González Pérez Coord. Depto. Editorial

### **Grupo Editor Ejecutivo**

Jorge Flores Troncoso, Editor en Jefe, UAZ México  
Manuel Reta Hernández, UAZ México  
Hamurabi Gamboa Rosales, UAZ México  
Claudia Sifuentes Gallardo, UAZ México

### **Grupo Revisor**

Oliver Joekisch, University of Applied Sciences, Germany  
Ding Hongwei, Tongji University, China  
Robert Weissbach., Penn State Erie, The Behrend College  
Naim Logic., Arizona Public Service  
Leonardo Acho Zuppa, U Politécnica de Catalunya, España  
Miguel Ándres, U. de Valencia, España  
Manuel Hernández Calviño, Universidad de La Habana, Cuba  
Luis C. García Santander, Universidad de Concepción, Chile  
Ramón Parra Michel, CINVESTAV, México  
Leonel Soriano Equigua, FIME-UCol, México  
Geminiano D. Martínez Ponce, CIO, México  
Carmen Maya Sánchez, CICESE México  
Jaime Sánchez García, CICESE México  
David H. Covarrubias Rosales, CICESE, México  
Enrique Pacheco Cabrera, AEM, México  
Remberto Sandoval Aréchiga, UAZ México  
Salavador Ibarra Delgado, UAZ México  
Rodrigo Soulé de Castro, UAZ México  
Ernesto García Domínguez, UAZ México  
Claudia Reyes Rivas, UAZ México  
Rafael Villela Varela, UAZ México  
Jorge de la Torre y Ramos, UAZ México  
Guillermo Romo Guzmán, UAZ México  
Rodrigo Castañeda Miranda, UAZ México  
Luis Octavio Sánchez Solís, UAZ México

## Contenido

---

Editorial	p. 1
Fabricación y Caracterización de Películas Delgadas de SiNx	pp. 2-6
A PHY LTE- Advanced analysis and a Software Defined Radio implementation	pp. 7-14

## Editorial

La revista *DIFU<sub>100</sub>ci@* es una revista cuatrimestral que comenzó su publicación oficial en 2005. En mayo del 2012, la revista *DIFU<sub>100</sub>ci@* adquirió el ISSN.

Desde entonces, se pretende contribuir a la difusión del conocimiento de la comunidad académica tanto nacional como internacional mediante la difusión de resultados de investigación de alta calidad. La Revista se centra en obras originales, que incluyen principalmente los estudios experimentales, análisis numéricos, estudios de casos y revisiones bibliográficas que proporcionan una significativa contribución a las áreas de ingeniería y tecnología en todas las disciplinas (Electrónica, Eléctrica, Ciencias de la Computación, Mecatrónica, Robótica, Telecomunicaciones, Procesamiento de señales, Ingeniería Industrial, Ingeniería de Control, y Bioingeniería).

Desde el comienzo, la revista ha buscado la mejora de los artículos aceptados para su publicación por un proceso de evaluación por pares o árbitro de los manuscritos recibidos. Estas evaluaciones son llevadas a cabo por expertos de reconocido prestigio por sus conocimientos y logros académicos, con el objetivo de asegurar que las publicaciones seleccionadas están contribuyendo al estado del arte en diferentes áreas de interés. Además, desde su inicio, la revista se ha abierto a los estudiantes y académicos a través del Sistema Open Journal, facilitando todo el proceso de presentación y publicación.

Agradezco a los autores y revisores, que se esfuerzan para mejorar la calidad de los manuscritos. Exhorto a todos los investigadores, académicos y estudiantes en las áreas de ingeniería y tecnología para que continúen sometiendo sus artículos en nuestra revista y contribuir a la noble difusión de la ciencia y la tecnología.

Jorge Flores Troncoso  
Editor en Jefe, Revista *DIFU<sub>100</sub>ci@*  
Universidad Autónoma de Zacatecas

# Fabricación y Caracterización de Películas Delgadas de SiNx

Jorge de la Torre y Ramos, Claudia Sifuentes Gallardo, Manuel Gámez Medina, María Teresa Torres Herrera,  
Jesús Manuel Rivas Martínez, Manuel Reta Hernández

Universidad Autónoma de Zacatecas, Unidad Académica de Ingeniería Eléctrica.  
Av. López Velarde 801, Col. Centro, Zacatecas, Zac., México, 98000.  
[jorgetorre@rocketmail.com](mailto:jorgetorre@rocketmail.com), [clausifuen@yahoo.com.mx](mailto:clausifuen@yahoo.com.mx)

2014 Published by DIFU<sub>100ci</sub>@ <http://www2.uaz.edu.mx/web/www/publicaciones>

## Resumen

En el presente trabajo se reporta la fabricación y caracterización de películas delgadas de nitruro de silicio por medio de la descomposición de silano ( $\text{SiH}_4$ ) y amoniaco ( $\text{NH}_3$ ), sobre diferentes sustratos como vidrio, silicio e ITO (óxido de indio dopado con dióxido de estaño); la deposición se lleva a cabo por medio de la técnica denominada deposición química en fase de vapor asistida por ultravioleta (UVCVD). Las características ópticas y eléctricas obtenidas indican un potencial interesante de este material para aplicaciones en celdas solares convencionales, incrementando la eficiencia de conversión, así como para celdas solares de tercera generación.

**Palabras clave:** Caracterización de películas delgadas, UVCVD, Películas delgadas de SiNx.

## 1. Introducción

Las predicciones referentes a la demanda de energía eléctrica tanto a nivel mundial como para México [1], indican un incremento continuo con la consecuente necesidad de búsqueda de alternativas, tanto económicamente viables, como ecológicamente sustentables. En este contexto, la energía solar fotovoltaica aparece como una de las fuentes de energía más promisorias, debido a la capacidad de convertir la luz del sol en electricidad sin producir emisiones de CO<sub>2</sub>. Sin embargo, la tecnología fotovoltaica presenta una desventaja importante en términos de costo por  $kWh$  generado con respecto a las otras tecnologías de generación convencionales, esto principalmente debido a la baja eficiencia de conversión que se sitúa entre 14 % y

16 % [2].

La tecnología actual de celdas solares fotovoltaicas está basada principalmente en el silicio en sus diferentes formas (monocristalino, policristalino y amorfo) como material de partida, representando más del 70 % del mercado actual. Sin embargo, el uso del silicio como material de base de las photoceldas implica un límite de rendimiento máximo del 31 % calculado según el modelo Schokley- Queisser [3]. Adicional al límite de rendimiento de conversión, la utilización de silicio provoca un costo elevado debido a que para la obtención del material de base se requiere material de alta pureza típicamente usado en la industria de la microelectrónica. Es por esto que la literatura [4] ha propuesto diferentes alternativas encaminadas, ya sea a aumentar el rendimiento o a disminuir el costo, tales como las celdas

a base de CdS/CdTe, CIS, a base de polímeros y celdas basadas en materiales nanoestructurados, sólo por mencionar algunas de las técnicas más importantes.

En el ámbito de las celdas a base de materiales nanoestructurados destaca el uso de nanoestructuras de silicio en una matriz de SiNx. La fabricación de dicho tipo de películas delgadas se ha basado principalmente en dos técnicas ampliamente utilizadas a nivel industrial que son el depósito químico en fase de vapor asistido por plasma (PECVD), y el depósito químico en fase de vapor a baja presión (LPCVD), teniendo ambos procesos el inconveniente de someter al material a tratamientos a altas temperaturas (mayores de 100°C).

En este trabajo se reporta la utilización de un sistema de depósito químico en fase de vapor asistido por luz ultravioleta (UVCVD) para la fabricación de capas nanoestructuradas de nitruro de silicio (SiNx) para su uso en celdas solares de la tercera generación. Los depósitos se realizan en tres diferentes sustratos: vidrio, silicio, y óxido de indio dopado con dióxido de estano (ITO). Finalmente, se reportan los resultados de la caracterización óptica y eléctrica de diversos depósitos realizados.

## 2. Detalles experimentales

### 2.1. Diseño del sistema

El sistema UVCVD se diseñó para el crecimiento de películas nanoestructuradas de SiNx en base al arreglo esquemático ilustrado en la figura 1.



Figura 1. Sistema de depósito UVCVD

Tabla 1. Condiciones generales para los depósitos

Característica	Valor
Tiempo	30 y 40 minutos
Relación de gases (SiH <sub>4</sub> /NH <sub>3</sub> )	0.5 y 1
Temperatura	60°C y 70°C
Substrato	Vidrio, Si-p < 110 >, ITO

Tabla 2. Condiciones utilizadas para los depósitos sobre silicio

Muestra	Temp. (°C)	Tiempo (min)	Relación de gases SiH <sub>4</sub> /NH <sub>3</sub> (sccm)
G1	70	30	50/100
G2	70	40	50/100
G3	60	40	50/100
G6	70	30	50/50

La cámara de reacción está construida con acero inoxidable con el fin de evitar que los gases utilizados para el depósito de material, como lo son el silano (SiH<sub>4</sub>) y el amoníaco (NH<sub>3</sub>), puedan degradar al reactor. Para controlar el flujo de los gases reactivos se utilizaron medidores de flujo tipo 092-04ST DWYER. La descomposición del silano requiere luz ultravioleta para lo cual se utilizó una lámpara UV modelo UVGL-58. Adicionalmente, el control de temperatura se realizó utilizando un controlador PID modelo AUTONICS TZN4S. Finalmente, el vacío necesario en la cámara de depósito se obtiene utilizando una bomba mecánica tipo ADIXEN SD2005.

Los depósitos se efectuaron a una presión de  $6 \times 10^{-2}$  mbar para condiciones variables como se describen en la tabla 1.

## 3. Resultados

### 3.1. Depósitos realizados

Para el sustrato de vidrio no se obtuvo depósito de material bajo ningún arreglo de parámetros.

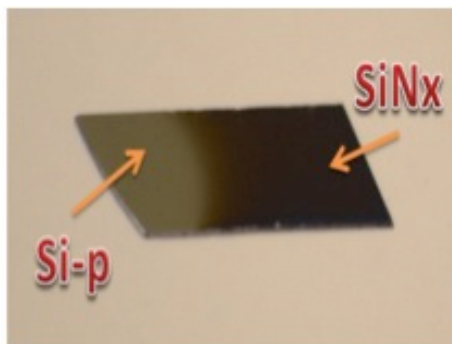
Para el caso del sustrato de silicio se obtuvieron depósitos con las condiciones descritas en la tabla 2.

Para el sustrato de ITO, en la tabla 3 se indican las condiciones para las cuales se obtuvo depósito de material.

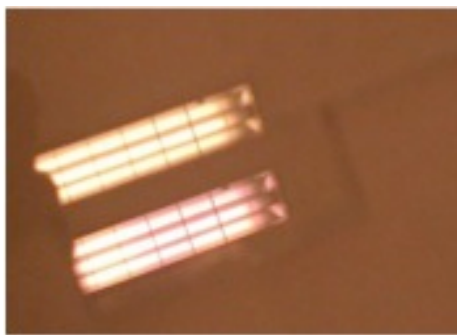
En la figura 2 se observan dos muestras depositadas sobre substratos de silicio e ITO, respectivamente. Se observan los cambios en el índice de refracción en

Tabla 3. Condiciones utilizadas para los depósitos sobre ITO

Muestra	Temp. (°C)	Tiempo (min)	Relación de gases SiH <sub>4</sub> /NH <sub>3</sub> (sccm)
ITO1	90	40	50/100
ITO2	120	40	50/100
ITO3	120	40	25/100
ITO4	120	20	25/100



(a) Substrato de silicio



(b) Substrato de ITO

Figura 2. Resultados de depósitos

ambos casos, siendo más evidente en los depósitos sobre silicio.

### 3.2. Caracterización óptica

Se llevó a cabo la caracterización óptica de algunas muestras obtenidas por medio de la técnica de fotoluminiscencia (PL). El banco de caracterización está constituido por un monocromador tipo Spectrapro 2300i, un fotomultiplicador Acton PD741 y una línea de excitación a 514 nm proveniente de una lámpara de Xenón tipo Acton.

La figura 3 presenta un espectro de fotoluminiscencia obtenido de la muestra G3. Se observan claramente hasta 3 bandas de emisión localizadas en 1.82 eV, 1.97 eV y 2.12 eV de las cuales se analizará su dependencia con respecto a los tres parámetros principales de depósito; es decir, temperatura del substrato, tiempo de depósito y relación de gases.

La figura 4 muestra el efecto de la variación en la relación de gases sobre la fotoluminiscencia. Se observa un corrimiento hacia las altas energías de la banda localizada a 1.75 eV al disminuir la relación de gases el cual pudiera indicar que el mecanismo de emisión asociado a dicha banda estaría asociado a nanoestructuras de silicio inmersas en la matriz de SiNx.

En la figura 5 se muestra el efecto de la variación del

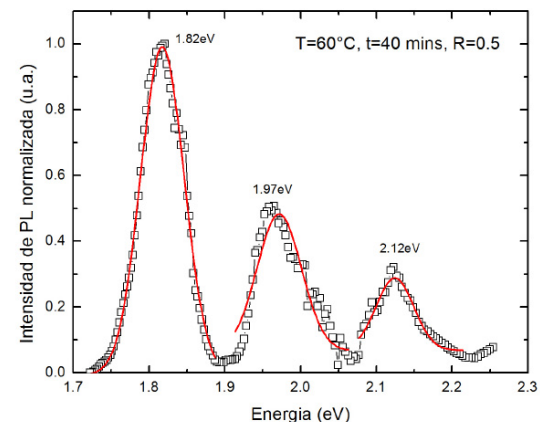
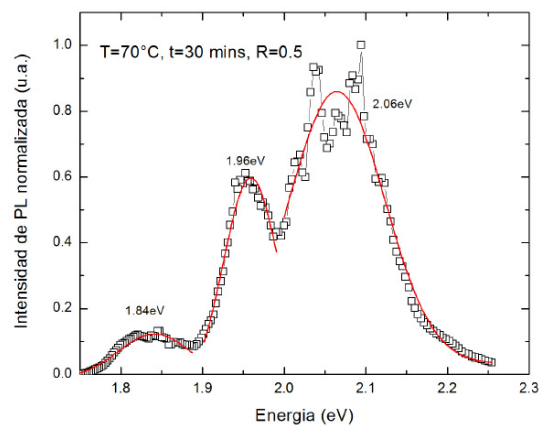
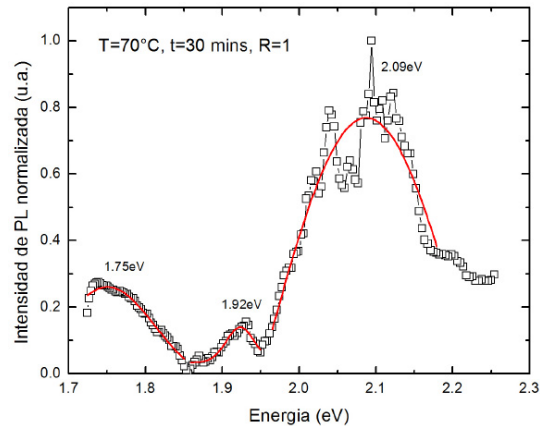


Figura 3. Espectro de PL obtenido de un depósito sobre substrato de silicio (muestra G3)

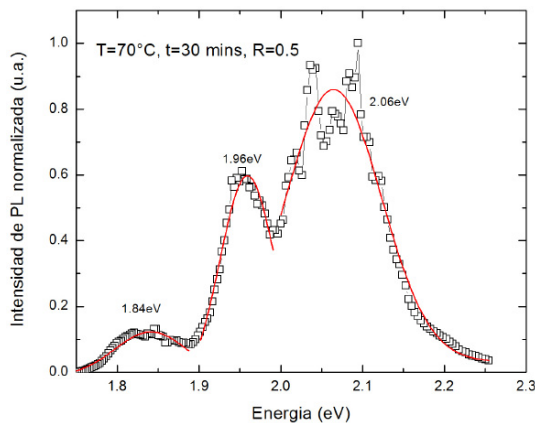


(a) Espectro de PL obtenido de la muestra G1

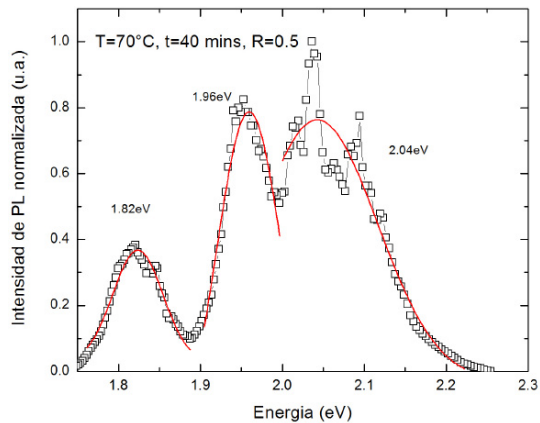


(b) Espectro de PL obtenido de la muestra G6

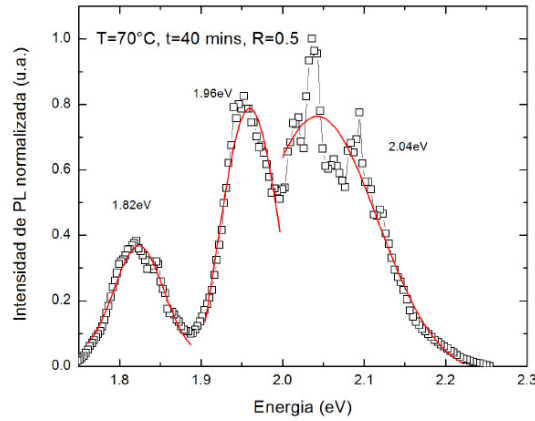
Figura 4. Espectros de PL obtenidos de las muestras G1 y G6 para analizar la influencia de la variación en la relación de gases sobre la PL.



(a) Espectro de PL obtenido de la muestra G1



(a) Espectro de PL obtenido de la muestra G2



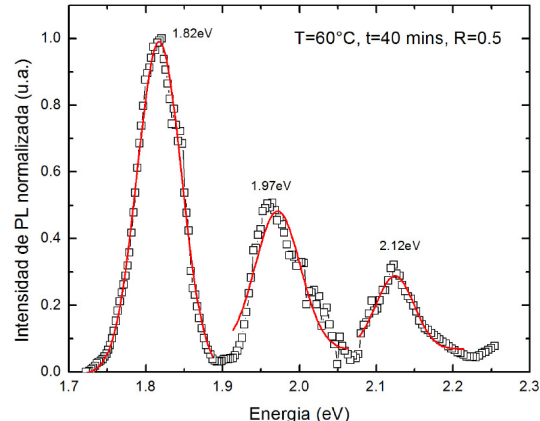
(b) Espectro de PL obtenido de la muestra G2

Figura 5. Espectros de PL obtenidos de las muestras G1 y G2 para analizar la influencia del tiempo de depósito sobre la PL.

tiempo de depósito, se observa que un incremento en el tiempo de depósito no altera la posición de las bandas de PL; sin embargo, sí altera la intensidad de la banda a 1.82 eV. Esto último estaría asociado a un aumento en la cantidad de material depositado al incrementar el tiempo de depósito provocando que exista una mayor cantidad de nanoestructuras y por consiguiente una intensidad de emisión de dicha banda mayor.

Finalmente, en la figura 6 se muestra el efecto de la temperatura del substrato sobre la PL. La posición energética de cada banda no se altera, solamente se observa un incremento en la intensidad relativa de emisión de la banda a 1.82 eV la cual aumenta con respecto a las otras bandas de emisión.

De los análisis de PL se puede concluir que la banda localizada a 1.82 eV estaría asociada a nanoestructuras de silicio inmersas en la matriz de SiNx, mientras que las bandas a 1.92 eV y 2.2 eV estarían más bien asociadas a defectos radiativos de la matriz SiNx, como se ha reportado en la literatura [5]. Sin embargo, hacen falta mayores estudios para corroborar estas observaciones.



(b) Espectro de PL obtenido de la muestra G3

Figura 6. Espectros de PL obtenidos de las muestras G2 y G3 para analizar la influencia del tiempo de depósito sobre la PL.

#### 4. Conclusiones

Se reporta el diseño y operación de un sistema de deposición de películas delgadas mediante la técnica de UVCVD. Se utilizaron tres tipos de sustratos vidrio, silicio e ITO para la fabricación de películas delgadas de SiNx. Los resultados preliminares muestran una banda de emisión fotoluminiscente posiblemente asociada a nanoestructuras de silicio inmersas en la matriz de SiNx. Este tipo de material posee gran potencial para aplicación en celdas solares de tercera generación así como para dispositivos electroluminiscentes.

#### Referencias

- [1] Secretaría de Energía. "Prospectiva del Sector Eléctrico Nacional 2013-2027", 2013. <http://www.sener.gob.mx>
- [2] T Markvart and L Casta. *Practical Handbook of Photovoltaics Fundamentals and Applications*, 1st Edition Elsevier, 2003, ISBN 1856173909.
- [3] W. Shockley and H.J. Queisser. "Detailed Balance limit of

- efficiency of pn junction solar cells". *J.Appl. Phys.*, Vol. 32, pp. 510, 1961.
- [4] D. Nikolic *et al*, "A review of silicon solar cells in photovoltaics technology". 7th International Quality Conference, pp. 213, 2013 .
- [5] H.L. Hao *et al*, "Origin of visible luminescence in hydrogenated amorphous silicon nitride". *Appl. Phys. Lett*, Vol. 91, pp. 201922-201922-3

# A PHY LTE- Advanced analysis and a Software Defined Radio implementation

Víktor Iván Rodríguez Abdalá<sup>a</sup>, Jaime Sánchez García<sup>a</sup>, Jorge Flores Troncoso<sup>b</sup>

<sup>a</sup>Centro de Investigación Científica y Educación Superior de Ensenada  
Carr. Ensenada-Tijuana 3918, Zona Playitas, Ensenada, B.C., México, 22860.

*{abdala, jasan}@cicese.edu.mx*

<sup>b</sup>Universidad Autónoma de Zacatecas, Unidad Académica de Ingeniería Eléctrica.  
Av. López Velarde 801, Col. Centro, Zacatecas, Zac., México, 98000.

*jflorest@uaz.edu.mx*

2014 Published by DIFU100ci@ <http://www2.uaz.edu.mx/web/www/publicaciones>

---

## Abstract

The capacity, reliability and services demand at high bit rates on cell phone communications are constantly demanding better performance, and together with the RF spectrum limitations force radio systems to achieve great spectral efficiency. In this article we analyze the physical layer (PHY) of the Long Term Evolution Advanced (LTE-A) standard that the workgroup 3GPP (3rd Generation Partnership Project) proposes as a solution to accomplish the 4G (Fourth Generation) compatibility requirements defined by the ITU-R (International Telecommunication Union) including up to 1 Gbps for downlink and 500 Mbps for uplink bit rates [1]. We describe the processes performed at the PHY layer in the uplink, and those stages where a free implementation is allowed to fully fill the 4G requirements.

**Keywords:** LTE-Advanced, 4G, SC-FDMA, uplink

---

## 1. Introduction

One of the keys to achieve higher bit transmission rates is the implementation and use of antenna arrays, which allows spatial multiplexing commonly known as MIMO (Multiple Input Multiple Output) and can be reinforced by the use of relays technique which consists in the transmission-reception of signals from-to users located into the cells to reduce the transmitter-to-receiver distance and thereby allowing for higher data rates [2].

Another key technique for achieving higher throughput in new generation networks is the so called OFDM (Orthogonal Frequency Division Multiplexing) air interface, which is based on the use of orthogonal subcarriers for data transmissions, where every symbol is transmitted in one subcarrier, minimizing multipath effects in the radio channel, achieving a better performance in joint with an efficient technique like MIMO.

A modification that has been done in the downlink access method is called OFDMA (Orthogonal Frequency Division Multiple Access) which allows to assign different

number of subcarriers to the mobile users (according to the needed transmission rate). Furthermore, SC-FDMA (Single Carrier - Frequency Division Multiple Access) has been proposed for the uplink. SC-FDMA allows a full orthogonal scheduled system (multiple users using a part of available carriers) with a low PAPR (Peak to Average Power Ratio) [3]. In the same way, a new technique is implemented on the PHY layer called Carrier Aggregation, which enables to transmit data at very high bit rates in a group of narrow bandwidth carriers, jointly achieving a higher capacity [4].

## 2. MAC and physical layer technologies (PHY)

### 2.1. Medium access methods (OFDMA and SC-FDMA)

The OFDMA technique was originally introduced as an air interface technology in the fixed wireless network IEEE802.16d standard in 2004; the IEEE802.16e standard was implemented in 2005 in order to allow users mobility in wireless networks. The adoption of the OFDMA technique on the PHY layer by 3GPP was done in 2005 as an evolution of WCDMA (Wideband CDMA) based on UMTS (Universal Mobile Telecommunications System). such modification is included in the standard refereed as 3GPP LTE Release 8 and it was finished in 2008. The new release of 3GPP standard is known as LTE Advanced Rel 10, which is actually being developed.

OFDMA permits the allocation of time/frequency resources to specific users, these divided on logical basic resource units which consist of subbands in frequency and one or more OFDM symbols in time domain. A subband comprises several subcarriers. The basic resource units are then mapped to the physical OFDMA frame, there exist two permutation schemes, the first one consist in distributing the data to transmit on noncontiguous subcarriers using the frequency diversity, achieving to reduce the error probability due to frequency selective fading or channel interference. In the second scheme, the data is sent in contiguous carriers, to allow multiuser diversity and frequency selective scheduling.

The PHY layer OFDMA implementation involves complications, like PAPR, which is particularly high in OFDM/OFDMA systems, because the OFDM symbol waveform in time domain is the superposition of sinusoids where the frequency is  $n$  times the lowest subcarrier. A high PAPR requires power amplifiers with a lineal output over a big frequency range. It is a factor that decreases the battery life and increases the cost in OFDMA mobile devices.

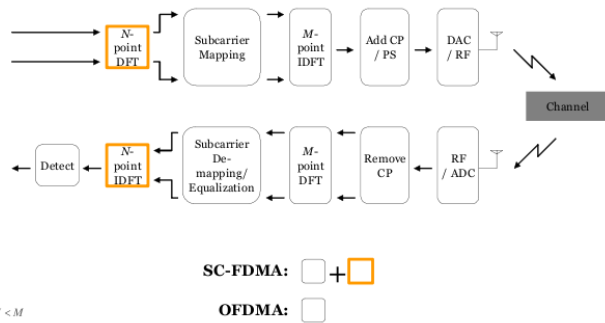


Figure 1. Block diagram of a OFDMA-SCFDMA system.

3GPP LTE-Advanced proposes to use a technology called SC-FDMA or DFTS-OFDM (Direct Fourier Transform Spread - OFDM) in the uplink, which among their main characteristics is the presence of a low PAPR. SC-FDMA technique consist in precoding the data symbol with a discret Fourier transform stage, as shown in Figure 1, and the samples obtained of the precoding stage are parallelly transmitted over a subcarriers group. The resulting time domain waveform have the characteristics of a single carrier waveform, with a low PAPR although the waveform is not a single carrier waveform [5].

The SC-FDMA transmitter handles blocks of size  $N$ , which contain the samples (complex values) of the digital modulated symbols, the  $N$ -point DFT stage generates a frequency domain representation of the input symbols. The samples are mapped in some of the  $M$  subcarriers available in the  $M$ -point IFFT stage, where  $M > N$ , transforming the subcarriers amplitude in a complex signal in the time domain. The value of  $N$  depends on the amount of users or the expansion factor  $Q$  and the amount of available subcarriers  $M$ , ( $N = M/Q$ ).

The samples obtained from the DFT stage are mapped in the corresponding subcarriers through two methods: distributed mapping of subcarriers and localized mapping of subcarriers. In the distributed mode (also known as DFDMA, Distributed Frequency Division Multiple Access), the DFT output is distributed over the subcarriers of all the available bandwidth, that is, on all necessary orthogonal subcarriers, and completing with zeros those subcarriers not utilized. In the localized mode (LFDMA) the DFT output is assigned to contiguous subcarriers, filling with zeros the higher and/or lower subcarriers.

In DFDMA, if the condition of  $M = Q \times N$  is accomplished, which means that, the occupied subcarriers are equidistant between them, the scheme is known as interleaving mode (IFDMA). It can be observed in Figure 2 why IFDMA is a special case of SC-FDMA, the implementation of the IFDMA technique becomes very

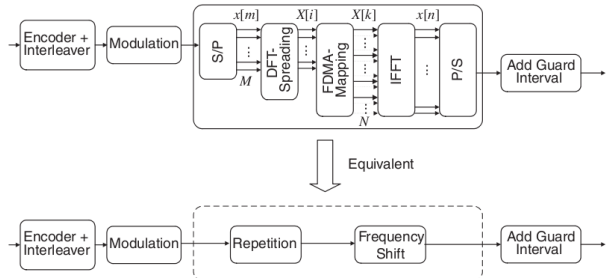


Figure 2. Equivalence of SC-FDMA and DFTS IFDMA in the uplink.

efficient because the SC-FDMA transmitter can modulate the signal strictly in time domain without the DFT and IFFT stages.

Depending on the mapping method, the modulated symbols of SC-FDMA can be different in time domain. For IFDMA, the modulated symbols in time are a repetition of the original input symbols, simply with a scaling factor of  $1/Q$  and some phase rotation. DFDMA and LFDMA have the same symbol structure in time and have exact copies of the symbols in time domain with a scaling factor of  $1/Q$  in the  $N$  positions of the samples and the intermediate values are the sum of all the symbols in time with different complex weight. For this reason there are more expected fluctuations and peaks in the amplitude of DFDMA and LFDMA [6].

## 2.2. Carrier Aggregation

The Carrier Aggregation technique allows to get together various LTE Carrier Components (CC) with an individual bandwidth of 20 MHz, until achieving a group with a 100 MHz bandwidth (up to 5 CC), and it can be observed as a separate CC of 100 MHz in the spectrum. The objective of grouping is to guarantee the compatibility with LTE devices, which requires a bandwidth of 20 MHz (LTE 8).

There are three configurations of Carrier Aggregation (CA): Contiguous CA, noncontiguous CA in the same band, and noncontiguous CA in different bands. The contiguous CA assigns to a LTE-A user a group of CC as a single CC, although a LTE user only see every CC individually. In case that several contiguous CC are not available, the noncontiguous CA configuration allows a LTE-A user to get the bandwidth required for the transmission. Due to the presence of two LTE users, the available CC are not contiguous, but the amount of all the CC unused in the band allows the bandwidth allocation required by the LTE-A user.

Also, in case that not enough CC exist to fullfill the bandwidth required by the LTE-A user, the CC available in other frequency band can be used, it is known as

noncontiguous CA in different bands. In noncontiguous CA in different bands scheme, a LTE-A user can present many different channel conditions due to the use of multiple bands with different frequencies, as well as different propagation delays between bands because of that it is connected to different base stations simultaneously [7].

## 2.3. Virtualization

The LTE-A transmitter includes the capacity to increase the diversity gain trough a transmission scheme of 8 antennas with only 4 physical antennas in the device. In this case, 4 virtual antennas may be added. In case of a  $6 \times 6$  array be desired, and just 4 physical antennas are available, two virtual antennas may be appended. This is possible with precoding and a small delay for mapping every diversity flow in a unique subgroup of physical antennas to conform a virtual antenna.

The LTE-A uplink transmitter can transmit two TB simultaneously. Besides it allows the transmission with a MIMO  $4 \times 4$  scheme through virtualization by the same way like the downlink transmitter, with precoding and a small delay for mapping every diversity flow in a unique subgroup of physical antennas to conform a virtual antenna.

## 3. Transmission structure

The transmission structure for downlink between the base station and users is defined by [8], where OFDMA is the medium access method technique. Due to the mobile device limitants (in both power and size), the uplink transmitter is designed with SC-FDMA as medium access method (MAC) technique. There are three types of logic channels for data transport, the broadcast channel (PBCH) used for transmitting the basic system configuration information; the multicast channel (PMCH) used for transmission services, like TV over a LTE infrastructure and the downlink shared channel (PDSCH) that is the main data channel, used to transmit data blocks known as transport blocks (TB), they are obtained from the MAC layer (Medium Access Control). In this standard, up to two TB can be transmitted simultaneously by an LTE-A user and downlink and uplink structure subframe using RB.

In the carrier aggregation case, the transmission over multiple subcarriers corresponds to multiple and diverse transport channels, and even to independent process on the PHY layer, like multiple transmitters in the same device to send data into multiple frequency bands.

According to [9], the PHY layer process includes the next stages:

1. 24 bits CRC insertion.
2. Channel coding: Turbo codes based on internal interleaving QPP (Quadratic Polynomial Permutation) with trellis termination.
3. PHY layer ARQ-hybrid process.
4. Channel interleaving.
5. Scrambling.
6. Digital modulation.
7. DFT precoding.
8. Layer mapping and precoding.
9. Mapping to antennas.

### 3.1. Code Block Segmentation and CRC attachment

A transport block (TB) is first segmented into multiple codeblock segments. There exists three CRC attachment schemes, in CRC attachment scheme 1, a CRC is computed for and attached to each segment independently. In scheme 2, CRC computation for the first codeblock segments is different from that for the last one. For the first segments, CRC is computed for and attached to each segment independently. The CRC bits attached to the last segment are computed based on all information bits of that transport block. In scheme 3, a TB-level CRC computed based on all information bits of that transport block is attached to the TB. The entire transport block along with the TB-level CRC is then segmented into multiple codeblock segments. A CRC is then computed for and attached to each segment independently. The two cyclic generator polynomials for  $L = 24$  referred to as gCRC24A ( $D$ ) and gCRC24B ( $D$ ) for transport block CRC and codeblock CRC respectively are given as:

$$\begin{aligned} gCRC24A(D) = & D^{24} + D^{23} + D^{18} + D^{17} + D^{14} \\ & + D^{11} + D^{10} + D^7 + D^6 + D^5 \quad (1) \\ & + D^4 + D^3 + D + 1. \end{aligned}$$

$$gCRC24B(D) = D^{24} + D^{23} + D^6 + D^5 + D + 1 \quad (2)$$

The first polynomial gCRC24A is used for transport block CRC calculation on UL-SCH, DL-SCH, PCH and MCH. The second polynomial gCRC24B is used for codeblock CRC calculation.

In LTE-A a minimum and maximum code block size is specified so the block sizes are compatible with the block sizes supported by the turbo interleaver, the minimum code block size is set to 40 bits and a maximum code block size equals to 6144 bits, if the length of the input block is greater than the maximum code block size the input block is segmented.

### 3.2. Turbo coding

The turbo coding used is a parallel concatenated convolutional code (PCCC) with two 8-state rate 1/2 constituent encoders and a “contention-free” Quadratic Permutation Polynomial (QPP) interleaver. The transfer function for each constituent encoder is given by:

$$G(D) = \left[ 1, \frac{g_1(D)}{g_0(D)} \right], \quad (3)$$

where

$$g_0(D) = 1 + D^2 + D^3, \quad (4)$$

$$g_1(D) = 1 + D + D^3. \quad (5)$$

The rate 1/3 turbo code generates a stream of systematics bits, a stream of parity bits from the first convolutional code (parity 1 bits) and a stream of parity bits from the second convolutional code (parity 2 bits).

The role of the interleaver in the second convolutional code input is to spread the information bits such that in the event of an error, the two codes are affected differently allowing data to still be recovered. The relationship between the output index  $i$  and the input index ( $i$ ) satisfies the following quadratic form:

$$\Pi(i) = f_1 \cdot i + f_2 \cdot i^2 \mod K, \quad (6)$$

where  $K$  is the number of input bits to the turbo code internal (QPP) interleaver,  $0 < i$  and  $f_1, f_2 < K$ . The common values of  $f_1$  and  $f_2$  are that the greatest common divisor of  $f_1$ , and  $K$  should be 1 and any prime factor of  $K$  should also divide  $f_2$ .

### 3.3. PHY layer ARQ-hybrid process

The bits input to the block interleaver are the bits for each of systematic, parity 1 and parity 2 streams. The interleaving is achieving by writing row-wise in a 32 column rectangular matrix, applying matrix columns permutations and finally reading from the matrix column-wise. The inter-column permutation for the matrix is performed based on the bit-reversal-order pattern, this is, for column 0001, the reversed bit number is 1000.

An additional interlacing is only performed between parity 1 and parity 2 bits, The systematic bits are not interlaced, This is to guaranteed an equal amount of parity 1 and parity 2 bits transmission.

### 3.4. Channel Interleaving

This subblock consists in a simple interleaver where bits are written to a rectangular matrix row-by-row and read out column-by-column .

### 3.5. Scrambling

The code bits delivered by the hybrid-ARQ functionality is multiplie (exclusive-or operation) by a bit-level scrambling sequence which consist in a unique ID cell. By applying different scrambling sequences for neighboring cells, the interfering signal after descrambling is randomized, ensuring full utilization of the processing gain provided by the channel code .

### 3.6. Digital modulation

The set of modulation schemes supported includes QPSK, 16QAM, and 64QAM, corresponding to two, four, and six bits per modulation symbol respectively.

### 3.7. DFT precoding

The modulation symbols, in blocks of  $M$  symbols, are fed through a size- $M$  DFT, where  $M$  corresponds to the number of subcarriers assigned for the transmission.

The DFT size should be constrained to a multiple of 12, from 12 up to 204, where the DFT can be implemented as a combination of relatively low- complex radix-2, radix-3, and radix-5 FFT processing. The DFT sizes of 60, 84, 120, 132, 156, 168, 180 and 204 will not be allowed .

### 3.8. Layer mapping and precoding

The complex symbols are mapped to one, two or four layers sequentially, this is, un case of two layer the even symbols are mapped to the first layer and the odd symbols are mapped to the second layer. In single mode, the symbols are mapped to one layer; in diversity mode, the symbols are mapped into two or four layers, depending on the number of transmit antennas used; in spatial multiplexing mode, the symbols are mapped into two, three or four layers, in this case the number of layers is always less or equal to the number of antennas used.

There exists three types of precoding, spatial multiplexing, transmit diversity and single antenna port transmission. Within spatial multiplexing there are two schemes; precoding with large delay Cyclic Delay Diversity (CDD), also known as open loop spatial multiplexing and precoding without CDD also known as closed loop spatial multiplexing.

For transmission over a single antenna port no processing is carried out over the symbols, for transmit diversity its employed an Alamouti scheme space-frequency for two and four antennas, for spatial multiplexing its employed a codebook configured by the eNodeB and user equipment when is required.

### 3.9. Mapping to antennas

The transmission scheme is based on a conventional OFDM transmitter. 7 OFDM symbols make a slot with a duration of 0.5 ms, a subframe is conformed by two slots, it corresponds to a TTI (Transmission Time Interval) with a duration of 1 ms. A radioframe takes 10 ms, so that, this is formed by 10 subframes or 10 TTI with a duration of 10 ms. The space between OFDM subcarriers is 15 kHz, where 12 subcarriers constitute a resource block (RB). The RB can contain from 6 up to 110 blocks. There are two kinds of cyclic prefix for the 7 OFDM symbols, the normal prefix of length  $160 \times T_s$  (for the first OFDM symbol), another one  $144 \times T_s$  (for the rest of OFDM symbols); and the extended prefix of  $512 \times T_s$  (for all OFDM symbols) where  $T_s = 1/(2048/15\text{kHz})$  which is the space between subcarriers. The system bandwidths are between 1.08 MHz (6 RB) up to 19.8 MHz (110 RB).

## 4. Transmission modes

LTE and LTE-A include the layer concept, which consists on assigning the transport blocks to the corresponding antenna for the transmission; it is worth to mention that the quantity of modulated symbols is the same, and equals the sum of the symbols to transmit in every antenna. There exist many transmission modes in LTE-A that indicate the way in which one or two transport blocks, after digital modulation, are mapped and processed to the different device antennas.

The transmission modes are:

**Transmission mode 1:** Single-antenna transmission.

**Transmission mode 2:** Transmit diversity.

**Transmission mode 3:** Open-loop codebook-based precoding in the case of more than one layer, transmit diversity in the case of rank-one transmission.

**Transmission mode 4:** Closed-loop codebook-based precoding.

**Transmission mode 5:** Multi-user-MIMO version of transmission mode 4.

**Transmission mode 6:** Special case of closed-loop codebook-based precoding limited to single-layer transmission.

**Transmission mode 7:** Release-8 non-codebook-based precoding supporting only single-layer transmission.

**Transmission mode 8:** Release-9 non-codebook-based precoding supporting up to two layers.

**Transmission mode 9:** Release-10 non-codebook-based precoding supporting up to eight layers.

These transmission modes are only applicable for sending DL-SCH.

In transmit diversity mode, the transmitter as well as the receiver use all the antennas to mitigate the multipath fading effects. This scheme is based in the Alamouti's space frequency block code (SFBC) and support two and four antennas.

When using transmit diversity mode, only a transmit TB per user is allowed, this is because the way the symbols are sent by the Alamouti's scheme, as shown in equation (7), the values for  $x_n$  are complex samples from a DFT precoding stage. The  $i$ th row is transmitted from the  $i$ th antenna, and each  $k$ th column is transmitted in the corresponding  $k$ th subcarrier. Subcarrier  $k_n$  is assigned by the IFFT stage inside an OFDM block.

$$\begin{bmatrix} x_1 & x_2 \\ -x_2^* & x_1^* \end{bmatrix} \quad (7)$$

For the configuration of four antennas, the Alamouti's code is defined by equation (8), where all the subcarriers are adjacent (columns).

$$\begin{bmatrix} x_1 & x_2 & & \\ -x_2^* & x_1^* & x_3 & x_4 \\ & & -x_4^* & x_3^* \end{bmatrix} \quad (8)$$

The spatial multiplexing mode, including both open-loop and closed-loop, are permitted by LTE-A, allowing every antenna to have an independent data flow. It must be mentioned that this mode is not standardized in 3GPP LTE Advanced Rel 10, allowing the free implementation of any algorithm for spatial multiplexing.

The basic procedure for codebook-based precoding consist in mapping the modulated symbols corresponding to one or two transport blocks in multiple layers. The quantity of layers are from one to the quantity of antennas presented in the device. The open-loop spatial multiplexing is intended for high mobility users, where the transmitter does not have knowledge of the channel. The precoding scheme used in this mode is based on CDD (Cyclic Delay Diversity), where a series of defined precoded matrices are applied in every RE (Resource Element); as a result, a frequency domain diversity is obtained, by the delay applied in every RE, even if the channel over the RE doesn't need it, as in a flat fading case [10].

The maximum possible throughput by LTE-A is obtained in spatial multiplexing closed-loop mode, but this technique requires the feedback of the channel state information at the transmitter (CSIT) and the user must have a low to medium mobility as well as a channel with medium to high SNR.

When the channel is perfectly known by the transmitter, the optimum scheme for spatial multiplexing is precoding by singular value decomposition (SVD) [11], which spatially decomposes the MIMO channel into virtual channels orthogonal among themselves.

## 5. Development in an USRP testbed with GNU Radio

The transmission capacity of LTE-A can achieve up to 3 Gbps; however, since we are using an USRP based testbed, the maximun data rate is restricted by the USB 2.0 interface. Actually, the USRP cards can sustain a 32 MBps data rate via USB 2.0. All samples sent over the USB interface are in 16-bit signed integers with IQ format; this means, 16-bit in-phase and 16-bit in-quadrature data where the data size is 4 bytes per complex sample. This results in a 8 MSps across the USB obtained from 32 MBps / 4 Byte. Since complex processing is used, this provides a maximum effective total spectral bandwidth of about 8 MHz, according to the Nyquist criteria [2].

GNU Radio is a free open source project of SDR for Python programming language, like a communication control plane, which allows the implementation of new Digital Signal Processing (DSP) blocks written in C++ programming language for critical and high performance processes in the data plane, it will allow to develop several routines that are not included in the actual GNU Radio project libraries. The stages like OFDM modulator, digital modulation and DFT spreading are performed with the available functions in GNU Radio libraries.

### 5.1. DFTS-OFDM Implementation

Figures 3 and 4 show a GNU Radio based implementation, the transmitter block diagram shows the bits generation, the CRC attachment, the header and payload bifurcation, their corresponding digital modulation (QPSK for header and 16-QAM for payload), the 192-points DFTS stage and the OFDM transmitter. The receiver shows a OFDM symbol detection stage based on Schmidl and Cox technique, when a symbol is detected the demux stage split the data flow into the header and payload stream, after the header is detected, the receiver has a channel state knowledge and performs the payload

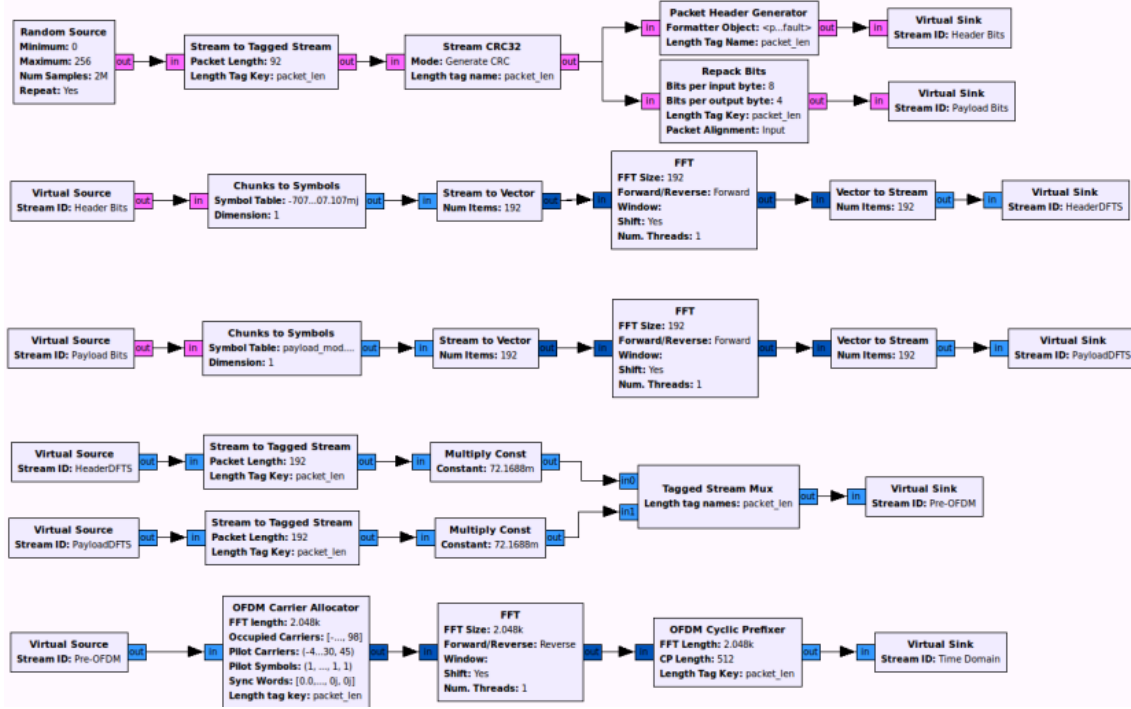


Figure 3. Block Diagram of a DFTS-OFDM SDR transmitter implementation.

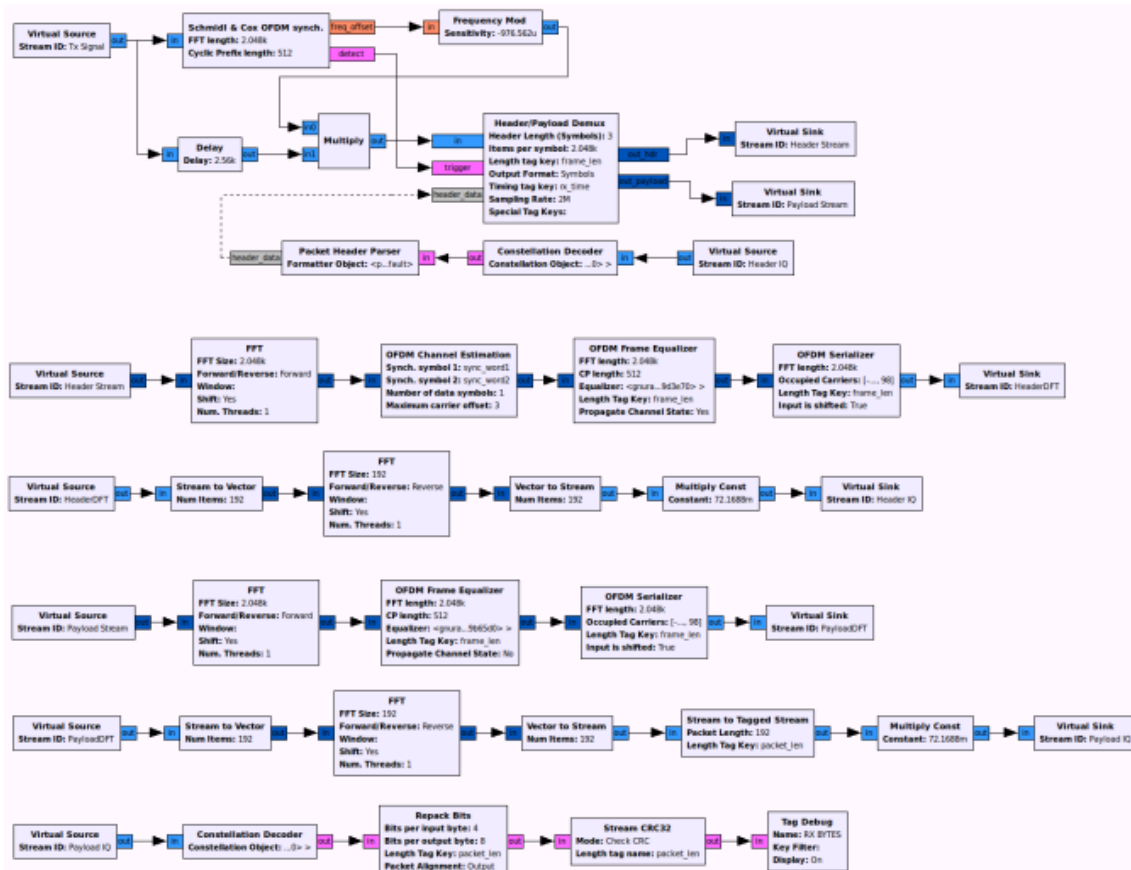


Figure 4. Block Diagram of a DFTS-OFDM SDR receiver implementation.

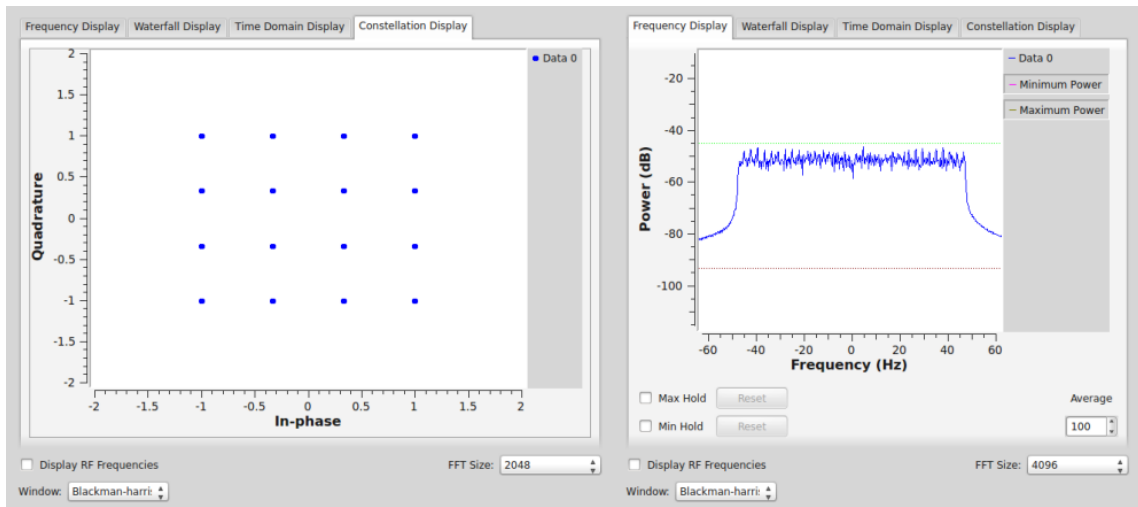


Figure 5. Implementation results.

recovery process, equalizing the OFDM symbol, applying a DFTS inverse process and finally demodulating the received signal. We can observe in Figure 5 an OFDM transmitted symbol and the payload constellation diagram at the receiver.

## 6. Conclusions and Future Work

This article is an overview of the stages that are part of the PHY layer of 3GPP LTE-A, where the implementation of SC-FDMA in mobile devices allows great battery power savings; the LTE-A standard also allows the use of a single OFDM symbol by many users at same time, by means of the OFDMA and SC-FDMA techniques for downlink and uplink respectively. The Carrier Aggregation technique (CA) offers to the mobile devices a bigger bandwidth (up to 100 MHz) by grouping different carrier components (CC). And the implementation of antenna virtualization (by precoding and a small delay) increases the transmissions modes up to 8x8 antenna array, which yields the freedom to implement multiple diversity techniques in the spatial, frequency and time domain.

Actually, we are developing a SDR project which allows an implementation of LTE-A PHY layer stages in a software environment called GNU Radio. The next step consists in developing the channel coding stages and perform a MIMO based communication between two or more USRP devices, to improve performance analysis with the aid of measurements.

## References

- [1] S. Parkvall, and E. Dahlman. "LTE-Advanced - Evolving LTE towards IMT-Advanced", *Vehicular Technology Conference (VTC 2008-Fall, IEEE 68th)*, 2008.
- [2] J. Parikh, and A. Basu. "LTE Advanced: The 4G Mobile Broadband Technology", *International Journal of Computer Applications*, Vol. 13, No. 5, January 2011.
- [3] S. Nagaraj, S. Garg, and F. Liang. "Lab Performance Analysis of a 4G LTE Prototype". *Wireless Communications and Networking Conference, WCNC 2009*, IEEE, 2009.
- [4] G. Yuan, and X. Zhang. "Carrier Aggregation for LTE-Advanced Mobile Communication Systems". *Communications Magazine*, February 2010.
- [5] A. Maeder, and N. Zein. "OFDMA in the Field: Current and Future Challenges". *ACM SIGCOMM Computer Communication Review*, Vol. 40, No. 5, October 2010.
- [6] H. G. Myung, "Introduction to Single Carrier FDMA". 15th European Signal Processing Conference (EUSIPCO 2007). Poznan, Poland. September 3-7, 2007.
- [7] I. F. Akyildiz, and D. M. Gutierrez-Estevez. *The evolution to 4G cellular systems: LTE-Advanced*. Physical Communication 3, pp. 217-244, 2010.
- [8] 3GPP TS 36.211 V8.0.0. 2007-09.
- [9] 3GPP TS 36.300 version 9.4.0 Release 9. ETSI, 2010.
- [10] CDD precoding for 4Tx antennas.. Technical Report R1-072019, 3GPP, 2007.
- [11] A. Goldsmith. *Wireless Communications*. Cambridge University Press, 2005.

